Lagrangian evolution of DMS during the Southern Ocean gas exchange experiment: The effects of vertical mixing and biological community shift

M. Yang,[1] S. D. Archer,[2] B. W. Blomquist,[3] D. T. Ho,[3] V. P. Lance,[4] and R. J. Torres[1]

[1] Concentrations of dimethylsulfide (DMS) and its precursor dimethylsulfoniopropionate (DMSP) are highly variable in time and space. What is driving the variability in DMS(P), and can those variability be explained by physical processes and changes in the biological community? During the Southern Ocean Gas Exchange Experiment (SO GasEx) in the austral fall of 2008, two ^{3}He/SF$_6$ labeled patches were created in the surface water. SF$_6$ and DMS were surveyed continuously in a Lagrangian framework, while direct measurements of air-sea exchange further constrained the gas budgets. Turbulent diffusivity at the base of the mixed layer was estimated from SF$_6$ profiles and used to calculate the vertical fluxes of DMS and nutrients. Increasing mixed layer nutrient concentrations due to mixing were associated with a shift in the phytoplankton community structure, which in turned likely affected the sulfur dynamics on timescales of days. DMS concentration as well as air-sea DMS flux appeared to be decoupled from the DMSP concentration, possibly due to grazing and bacterial DMS production. Contrary to expectations, in an environment with high winds and modest productivity, physical processes (air-sea exchange, photochemistry, vertical mixing) only accounted for a small fraction of DMS loss from the surface water. Among the DMS sinks, inferred biological consumption most likely dominated during SO GasEx.

1. Introduction

[2] Dimethylsulfide (DMS) is largely a product of microbiological activities in the surface ocean, with a global sea-to-air flux of 17.6~34.4 Tg S yr^{-1} [*Lana et al.*, 2011]. It is the largest biogenic contributor to sulfur aerosols, which can affect the radiative properties and chemistry of the marine atmosphere [*Charlson et al.*, 1987, 1992]. Predicting DMS emission rates and quantifying its climatic impact, however, have proven to be challenging, partly due to complexities in the surface ocean biological sulfur cycle.

[3] Dimethylsulfoniopropionate (DMSP), the precursor to DMS, makes up the bulk of the reduced sulfur pool in marine systems [*Simó and Dachs*, 2002] and may have osmotic [*Dickson and Kirst*, 1986] and antioxidant func-

tions [*Sunda et al.*, 2002]. Algal DMSP content (DMSP$_p$) is highly species-specific, with prymnesiophytes containing much higher concentrations than diatoms [*Keller et al.*, 1989]. The enzyme-catalyzed cleavage from DMSP to DMS occurs both within algal cells (i.e., from DSMP$_p$) and in seawater by bacteria (i.e., from dissolved DMSP, or DMSP$_d$). DMSP and DMS are released from phytoplankton to the water column mainly due to stress such as elevated ultraviolet radiation (UVR) and low nutrient availability [*Archer et al.*, 2010]. Zooplankton grazing of phytoplankton leads to cell rupture, which further enhance the release of DMS(P) [*Dacey and Wakeham*, 1986]. Despite its algal origin, peak concentration of DMS is often observed during the decline of a phytoplankton bloom rather than the active growing phase. One reason for this time lag could be the bacterial control on DMS production [*Polimene et al.*, 2012]. Not all DMSP is converted to DMS. The majority of DMSP$_d$ is microbially demethylated to form methanethiol—likely an important source of reduced sulfur for bacteria [*Kiene*, 1990; *Kiene and Linn*, 2000].

[4] Bacterial consumption, air-sea exchange, and photochemically mediated destruction are the three major sinks of DMS in the water column. From the eastern tropical Pacific and the northeastern Pacific, bacterial turnover for DMS was observed to be much faster than air-sea exchange [*Kiene and Bates*, 1990; *Bates et al.*, 1994]. A similar conclusion was reported by *del Valle et al.* [2009] for the Ross

[1]Plymouth Marine Laboratory, Prospect Place, Plymouth, Devon, UK.
[2]Bigelow Laboratory for Ocean Sciences, East Boothbay, Maine, USA.
[3]Department of Oceanography, University of Hawaii, Honolulu, Hawaii, USA.
[4]Lamont-Doherty Earth Observatory at Columbia University, New York, USA.

Correspondence author: M. Yang, Plymouth Marine Laboratory, Prospect Place, West Hoe, Plymouth, Devon PL1 3DH, UK. (miya@pml.ac.uk)

Sea, Antarctica. From the subtropical North Atlantic, *Toole et al.* [2006] found photochemistry to be the largest DMS sink for a shallow mixed layer (ML), while biological consumption became more important when the ML deepened. During the austral summer with high light dose, *Toole et al.* [2004] found photochemistry to be the dominant sink of DMS in the Ross Sea.

[5] The aforementioned budget studies were all based on an Eulerian framework, whereas a more accurate characterization of seawater DMS cycling necessitates a Lagrangian approach. *Simó and Pedrós-Alió* [1999] followed an anticyclonic eddy in the subpolar North Atlantic during a coccolithophore bloom. They found that microbial consumption and photochemistry each accounted for ∼45% of the DMS loss, while sea-to-air emission estimated from a wind speed dependent gas exchange parameterization contributed to ∼10%. *Archer et al.* [2002] tracked water dominated by coccolithophores in the North Sea for 6 days and found bacterial consumption to be the largest DMS sink for surface waters (∼70%), followed by photochemistry (∼20%), and gas exchange (∼9% for an intermediate transfer velocity parameterization). More recently, *Bailey et al.* [2008] reported measurements following a cyclonic and an anticyclonic eddy in the subtropical North Atlantic. They found nearly equal contributions to DMS loss from bacterial consumption, photochemistry, and gas exchange—the latter measured directly with eddy covariance. In their case, because higher production and concentration of DMS were found at depth, vertical mixing at the base of the ML increased the surface DMS concentration as well as nutrient supply, thereby influencing the biology.

[6] In this paper, we describe the evolution of seawater DMS during the Southern Ocean Gas Exchange Experiment (SO GasEx). Near surface DMS concentration was measured continuously in two ^{3}He/SF$_6$ patches, representing one of the most comprehensive coverage of DMS concentration measurements both for a Lagrangian framework and in the Southern Ocean. There have been a number of SF$_6$ tracer studies in the Southern Ocean, but all with simultaneous deliberate iron additions [*Boyd et al.*, 2007]. SO GasEx represents the first "unperturbed" tracer study in the Southern Ocean with measurements of sulfur compounds. Direct quantification of air-sea DMS flux by eddy covariance and estimates of vertical mixing from SF$_6$ robustly constrain the physical environment. Contrasting Patch 1 (net autotrophic) with Patch 2 (net heterotrophic to slightly autotrophic) [*Hamme et al.*, 2012], we examine the magnitude of the net biological processes in DMS cycling as well as the linkage between biology and physics.

2. Site Description and Patch Evolutions

[7] SO GasEx took place between February and April 2008 in the southwest Atlantic sector of the Southern Ocean near South Georgia, on board the NOAA ship *Ronald H. Brown* [*Ho et al.*, 2011a]. Two ^{3}He/SF$_6$ tracer patches were created within the Antarctic Zone (AZ) between the Antarctic Polar Front and the SubAntarctic Circumpolar Current Front [*Orsi et al*, 1995]. Based on underway SF$_6$ concentration data (every minute from ∼5 m depth), Patch 1 was followed from 10 March to 14 March and Patch 2 from 21 March to 5 April [see contours from
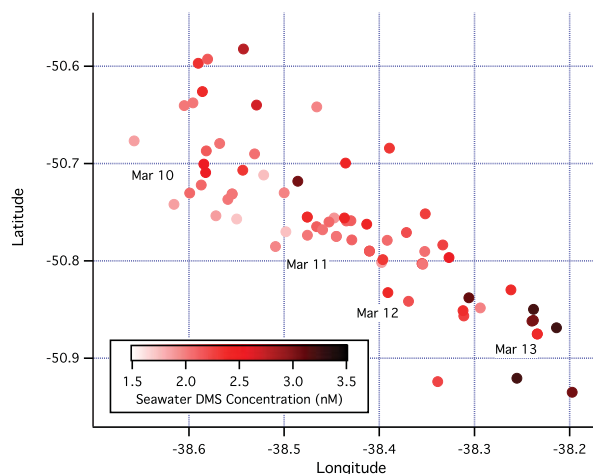

Figure 1. Map of Patch 1 color-coded by hourly seawater DMS concentration and marked on selected dates. Significant variability was observed over spatial scales of a few kilometers, while the range in DMS concentration during the duration of the patch was about a factor of two.

Ho et al., 2011a]. The methodology for SF$_6$ analysis has been described by *Ho et al.* [2011b]. CTD casts were made twice a day (around noon and midnight, local time) near the patch center, providing depth profiles.

[8] Underway DMS concentration was measured every ∼10 min from the ship's nontoxic water supply. The system consisted of a membrane equilibrator linked to a cold adsorbent trap and a Varian 3800 Gas GC with a pulsed flame photometric detector [see *Yang et al.*, 2011 for more details]. Discrete DMS samples were also taken from the CTD and measured using a purge system linked to the same cold-adsorbent trap as the underway system. Also from the CTD, samples for total DMSP (which largely comprises DMSP$_p$ but includes a component of DMSP$_d$ of the order of 5%) were fixed with sulfuric acid [*Kiene and Slezak*, 2006] and stored until analyzed as DMS following alkaline hydrolysis using the same purge and adsorbent trap system. The equilibrator system was calibrated and sensitivity monitored each hour using a permeation device (Dynacal®, Vici Metronics Inc.) delivering 120 ng DMS min^{-1} at 30°C. The purge and trap-based system was calibrated using a DMSP-HCl standard (>98% purity; Centrum voor Analyse, Spectroscopie and Synthese, Rijksuniversiteit Groningen).

2.1. Near Surface Concentrations

[9] Figures 1 and 2 show the distributions of seawater DMS concentration for the two tracer patches, which demonstrated significant spatial and temporal variability. For Patch 1 (Figures 1 and 3), DMS concentration (mean of 2.2 nM) was variable but showed a slight increase with time. DMSP concentration (mean of 63 nM) also built up over the 4 days, while chlorophyll a (Chl*a*) from high performance liquid chromatography (from CTD) remained relatively constant [*Lance et al.*, 2012]. The DMS:DMSP ratio was around 0.03, much lower than in Patch 2. Sea-to-air flux largely followed the trend of wind speed, except for midday on 10 March and the end of 13 March, when seawater DMS concentrations changed substantially. For Patch
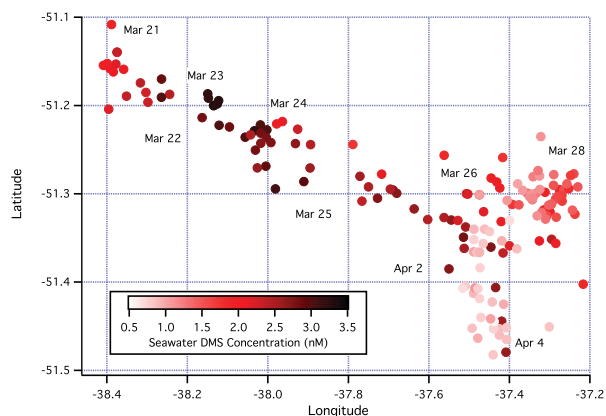
Figure 2. Map of Patch 2 color-coded by seawater DMS concentration and marked on selected dates. Over 2 weeks, the range in DMS concentration change was about a factor of five.

2 (Figures 2 and 4), DMS concentration increased rapidly from ∼2 nM on 21 March to over 3 nM by 24 March, and steadily declined thereafter to under 1 nM. Maximum DMS concentration coincided with elevated values of DMSP as well as Chl*a*. However, with an average of ∼22 nM, DMSP concentration did not demonstrate a similar decrease to DMS. The DMS:DMSP ratio varied similarly to DMS concentration (range of 0.02∼0.15), whereas DMSP:Chl*a* (in nmol μg⁻¹) steadily increased. DMS flux followed the same pattern as seawater DMS concentration, peaking on 24 March and decreasing over the rest of the patch duration, despite several high wind events. Atmospheric DMS concentration did not show a similar trend to seawater concentration and flux on this temporal/spatial scale, presumably due to photochemistry and atmospheric transport (e.g., the opposite of what was observed by *Yang et al.* [2009]). Often cloudy, the daytime shortwave irradiance measured by a shipboard radiometer at 18 m AMSL varied between 100 and 500 W m⁻².

2.2. Mixed Layer Properties

[10] Examples of depth profiles of DMSP and DMS near the beginning and end of Patch 2 are shown in Figure 5. DMS concentration on 3 April was less than half of the concentration on 22 March, whereas DMSP concentration increased slightly. The bulk of both sulfur compounds resided within the ML (∼50 m for these casts); below 75 m, the concentrations of DMSP and DMS for Patch 2 averaged 4.5 and 0.2 nM, respectively. Two operationally defined mixed layer depths (MLD) are given by *Ho et al.* [2011a]. The depth where the density was at least 0.01 kg m⁻³ greater than the density at 5 dbar (MLDρ) was generally shallower than the depth where the SF$_6$ concentration was half of its average concentration in the top 20 m (MLD$_{SF6}$). In particular, on 12 March and from 26 March to 28 March, strong solar irradiance resulted in a much shallower MLDρ; yet MLD$_{SF6}$ remained largely unchanged. Turbulent mixing was likely reduced during these periods of increased stratification. As noted by *Ho et al.* [2011a], MLDρ may be more closely related to the depth above which mixing was active, whereas MLD$_{SF6}$ indicates the depth of the already well-mixed layer, which

appears to be more consistent with vertical profiles of DMS and DMSP.

[11] For Patch 1, MLDρ and MLD$_{SF6}$ scattered around 37 and 49 m but did not show a significant temporal trend. The mixed layer deepened with time during Patch 2 [*Ho et al.*, 2011a], with mean MLDρ and MLD$_{SF6}$ of 49 and 59 m, respectively. However, MLD varied significantly from cast to cast, likely due to the propagation of internal waves on times scales of half a day [*Moore et al.*, 2011; *Hamme et al.*, 2012]. For Patch 2, separate linear fits of MLD$_{SF6}$ with time prior to and after the storm resulted in low correlations (r^2 of 0.1 and 0.3, respectively). To remove the effect of internal waves, we first determine the density corresponding to where SF$_6$ concentration was half of the surface value (Figure 6). These densities are then converted back to depth units using the mean depth versus density relationship (Appendix Figure A1). Linear fits of these depths over time result in ML deepening rates of 1.0 and 1.6 m d⁻¹ before and after the storm, with now much higher r^2 values of around 0.9 (Appendix Figure A2). However, this apparent deepening of ML might not have been entirely due to vertical mixing, as the isopycnals also shoaled over time at an approximate rate of 0.5 m d⁻¹. Below, we first estimate the vertical turbulent diffusivities from SF$_6$ profiles and then apply them to DMS and nutrients. Patch 2 was followed for a longer duration than Patch 1, allowing for more accurate determination of mixing rates. We thus primarily use Patch 2 to demonstrate our budget analyses.

3. SF$_6$ Budget

[12] Primarily of anthropogenic in origin and nonreactive in seawater, SF$_6$ has often been used as a conservative tracer [e.g., *Wanninkhof et al.*, 1997]. Its rate of change over time in the mixed layer is only affected by physical processes:

$$\frac{\partial \langle SF_6 \rangle}{\partial t} = -F_{SF6} + E_{SF6} - H_{SF6} \qquad (1)$$

[13] All terms above have units of flux. $\langle SF_6 \rangle$ on the left-hand side (LHS) of equation (1) is the ML integrated concentration at patch center, derived from multiplying locally maximum surface concentrations (SF$_{6,0}$) by MLD$_{SF6}$. This removes the dilution effect due to changes in the MLD. The three terms on the right-hand side (RHS) represent the sea-to-air flux, vertical mixing, and horizontal dilution, respectively. Following the initial release of Patch 2, SF$_6$ concentration decreased exponentially over the 2 week period, as expected for first-order dilution. Below we explicitly estimate each loss term on hourly intervals, and then examine the entire SF$_6$ budget for Patch 2.

3.1. Sea-to-Air Flux of SF$_6$

[14] We calculate the sea-to-air flux of SF$_6$ at patch center from the transfer velocity of SF$_6$ (k_{SF6}) and the air-sea concentration difference:

$$F_{SF6} = k_{SF6}(SF_{6,0} - \alpha_{SF6} \cdot SF_{6,atm}) \qquad (2)$$

[15] Here k_{SF6} is the transfer velocity of SF$_6$; α_{SF6} is the solubility of SF$_6$ as a function of temperature and salinity
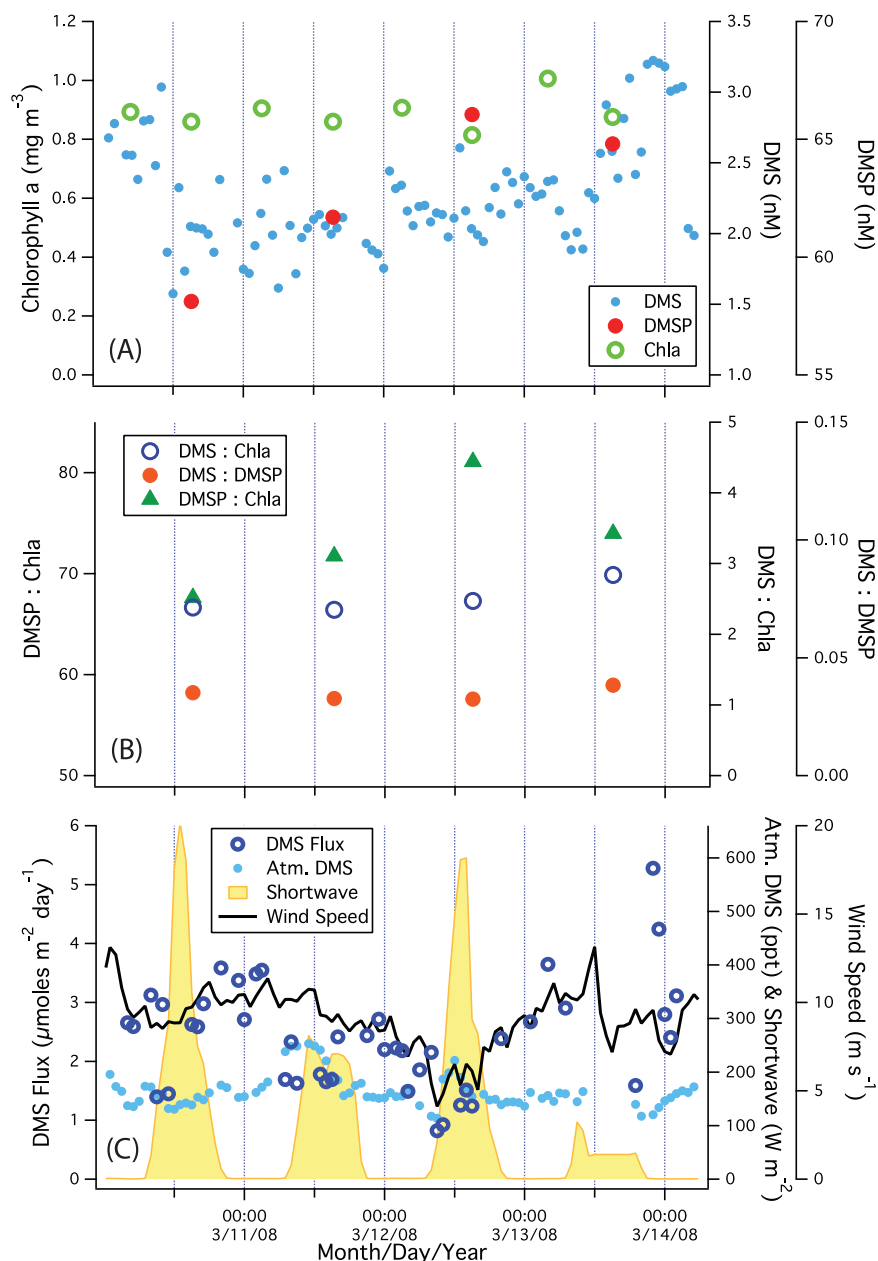
Figure 3. Time series of near-surface concentrations of (a) DMS, DMSP, and Chl*a*; (b) ratios among them; (c) DMS sea-to-air flux, atmospheric DMS concentration, wind speed, and shortwave irradiance (18 m AMSL) from Patch 1. Seawater DMS and DMSP concentrations increased slightly over the 4 days, while Chl*a* remained relatively constant. DMS flux largely followed the trend in wind speed.

[*Wanninkhof*, 1992]; $SF_{6,atm}$ is the atmospheric concentration. We assign $SF_{6,atm}$ to 6 pptv based on ambient measurements on four different days during SO GasEx, in agreement with the mean value from the Southern Hemisphere at that time (http://www.esrl.noaa.gov/gmd/hats/combined/SF6.html). This $SF_{6,atm}$ corresponds to a surface water equilibrium concentration of ~2 fmolar (fM) at ambient temperature, consistent with background values below the ML (>75 m depth) for most casts.

[16] From the change in $^3He/SF_6$ over several days following the patch, the gas transfer velocity for sparingly soluble gases was derived [*Ho et al.*, 2011b], which is consistent with the wind speed relationship previously

described by *Ho et al.* [2006]. To generate a time series of k_{SF6} at a higher time resolution than was measured during the project, we compute k_{SF6} using the wind speed parameterization from *Ho et al.* [2006]:

$$k_{SF6} = 0.266 U_{10n}^2 \left(\frac{Sc_{SF6}}{600} \right)^{-1/2} \qquad (3)$$

[17] Here U_{10n} is the hourly 10 m wind speed measured by a sonic anemometer and corrected for atmospheric stability; Sc_{SF6} is the Schmidt number of SF_6 [*King and Saltzman*, 1995], which is around 2300 for SO GasEx. The term inside the parenthesis accounts for the diffusivity
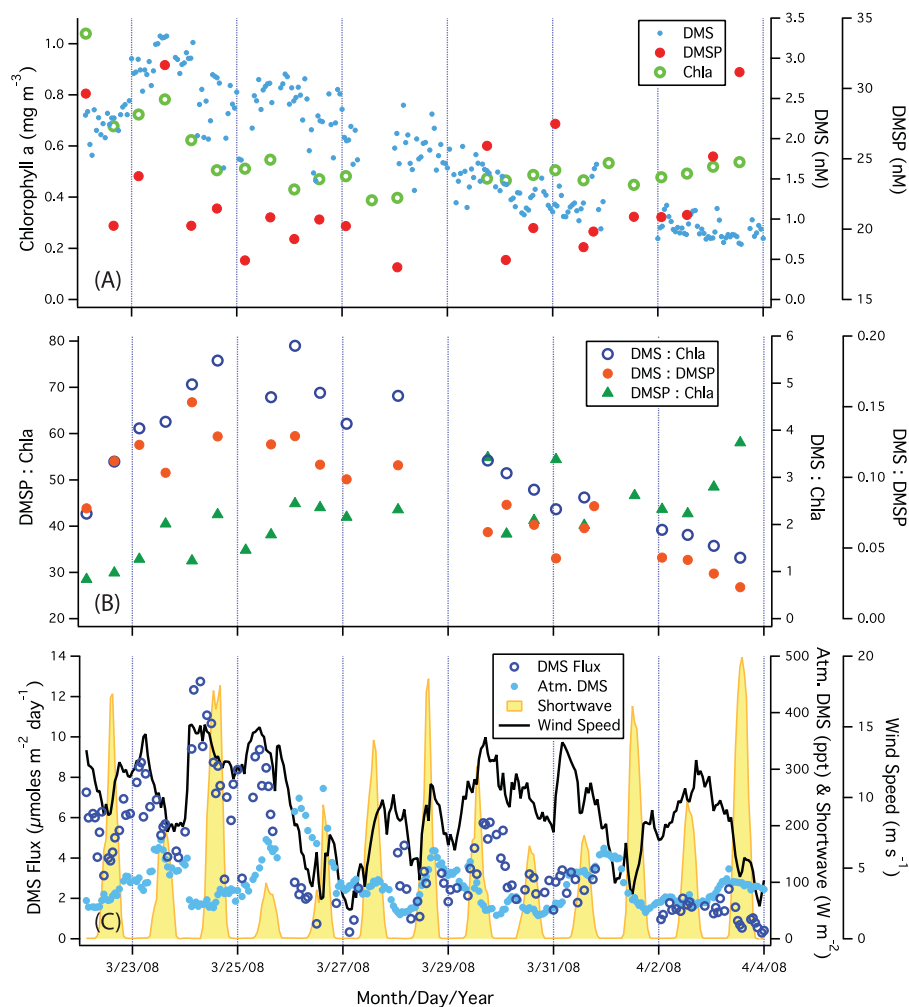
Figure 4. Time series of near-surface concentrations of (a) DMS, DMSP, and Chl*a*; (b) ratios among them; (c) DMS sea-to-air flux, atmospheric DMS concentration, wind speed, and shortwave irradiance (18 m AMSL) from Patch 2. The seawater DMS:DMSP ratio varied in a similar fashion to DMS concentration, while DMSP:Chl*a* steadily increased during Patch 2. DMS flux decreased during the latter stage of Patch 2 due to reduced seawater DMS concentration, despite some high wind speed episodes. DMS concentration in air, affected by photochemistry and atmospheric transport, did not demonstrate a systematic decrease as with concentration in water.

dependence in transfer velocity as a function of temperature and salinity. Overall, air-sea exchange explains ~18% of the SF_6 loss for Patch 2.

3.2. Vertical Mixing of SF_6

[18] Turbulent diffusivity in the vertical (K_z) is usually orders of magnitude smaller than in the horizontal due to stratification [*Ledwell et al.*, 1993]. In the open ocean, internal waves and surface forcing lead to turbulence in the pycnocline at the base of the ML [*Gregg*, 1987]. Elevated K_z there can result in a deepening of the ML via entrainment of water from below, with the vertical scalar flux parameterized as K_z multiplied by the gradient in scalar concentration. Here we estimate K_z by fitting vertical profiles of SF_6 with the complementary error function, as described by *Law et al.* [2003].

[19] To remove the heaving effect from internal waves, we first reference the measured CTD depths to the mean density-depth relationship. For each CTD cast near the center of the SF_6 patch, a fit to the concentration profile (SF_6 (z_c,t)) at density-corrected depth (z_c) is calculated above and below the target ML (Z_{ML}):

$$\frac{SF_6(z_c, t) - SF_{6,\infty}}{SF_{6,0} - SF_{6,\infty}} = \begin{cases} 1 & (z_c \leq z_{ML}) \\ erfc\left(\frac{z_c - z_{ML}}{\sigma}\right) & (z_c > z_{ML}) \end{cases} \quad (4)$$

[20] $SF_{6,\infty}$ represents the background concentration below 100 m. Typically around 2 fM, $SF_{6,\infty}$ was occasionally elevated (e.g., ~7 fM for Cast 40), possibly due to advection of a previously labeled water mass. Numerically similar to $SF_{6,0}$, $SF_{6,ML}$ is the average concentration within the mixed layer. The complementary error function (erfc) function has the form:
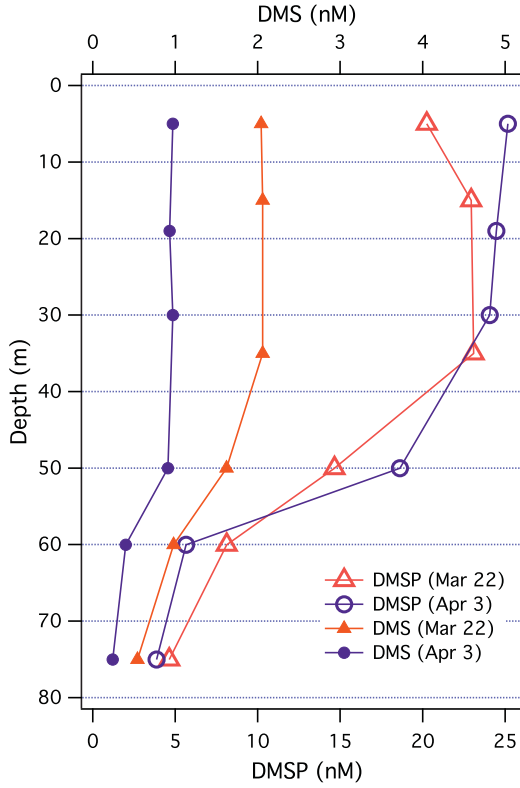
Figure 5. Profiles of DMSP and DMS near the beginning and end of Patch 2. DMS concentration toward the end of the period was less than half of the initial value, while DMSP concentration showed a small increase.

$$\mathrm{erfc}\,(x) = 1 - \frac{2}{\sqrt{\pi}} \int_0^x e^{-\beta^2}\,d\beta \qquad (5)$$

[21] The width scale σ is in units of meters and varies with K_z as well as time:

$$\sigma = 2\sqrt{K_z t} \qquad (6)$$

[22] The erfc fitting for each profile is optimized using a least-squared method at a given set of Z_{ML} and σ, which are not known a priori. Related to the "target isopycnal" where diapycnal mixing is expected to occur [*Ledwell et al.*, 1993], Z_{ML} of 53 m appears to satisfy the least total errors for all days considered and is thus kept constant for the fittings of all profiles for Patch 2 (see Appendix A1 for more details). For reference, on the first cast following the tracer release on the morning of 22 March, the density where $SF_{6,n} = 0.5$ corresponds to $\sim$54 m based on the mean density-depth relationship, while MLD_{SF_6} and $MLD\rho$ without density correction were 60 and 46 m, respectively.

[23] The fitted SF_6 profiles at this Z_{ML} are shown for 3 days prior to and after the storm in Figure 7. From equation (6), linearly fitting the prestorm and poststorm days separately leads to K_z of 0.4 ± 0.2 and 0.9 ± 0.3 cm^2 s^{-1}, respectively, while fitting over the entire Patch 2 period leads to $\sim$0.6 cm^2 s^{-1} (Figure 8a). The uncertainties above indicate the errors in curve fitting. An alternate approach using the second moment yielded a similar K_z value of

$\sim$0.5 cm^2 s^{-1} (Figure 8b), which is discussed in Appendix A1. We did not attempt to use SF_6 profiles between 26 and 28 March, as the mixed layer shoaled briefly following the storm and the SF_6 profiles did not follow the erfc form. Using the same approach, K_z was estimated to be 0.3 ± 0.3 cm^2 s^{-1} for Patch 1. Compared to Patch 2, the lower K_z for Patch 1 is consistent with the relatively constant MLD (no obvious deepening).

[24] Knowing K_z, the vertical flux of SF_6 at the base of the mixed layer is simply:

$$E_{SF6} = K_Z(\Delta SF_6/\Delta z) \qquad (7)$$

[25] We estimate the concentration jump ΔSF_6 from CTD profiles and Δz as the thickness of the pycnocline (typically 8$\sim$10 m) from the high resolution (1 m) density data. Using K_z of 0.4 cm^2 s^{-1} for the prestorm period and 0.9 cm^2 s^{-1} for the poststorm period, vertical mixing accounted for $\sim$2% of the decrease in SF_6 concentration for Patch 2.

3.3. Horizontal Dilution of Tracer Patch

[26] As shown by *Ho et al.* [2011a], Patch 2 became enlarged, elongated, and advected to the southeast over time. We can determine the horizontal spreading rate from the increase in patch area. In practice, this is complicated by the fact that the ship often surveyed the same region at different times while the patch drifted, resulting in an apparent patch area that is larger than the actual size. To separate space from time, we first divide the SF_6 underway data into daily intervals. The geographical coordinates are then corrected for horizontal advection using the mean daily ADCP velocity from the shallowest bin at 25 m. Daily contours are generated based on advection-corrected
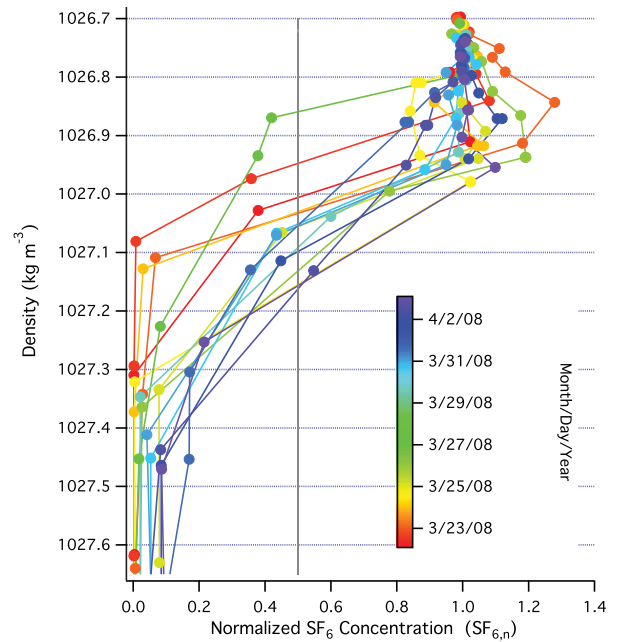

Figure 6. Profiles of SF_6 concentration normalized to the surface value as a function of density for Patch 2, color-coded by time. The increase in density where $SF_{6,n} = 0.5$ illustrates the gradual deepening of the ML.
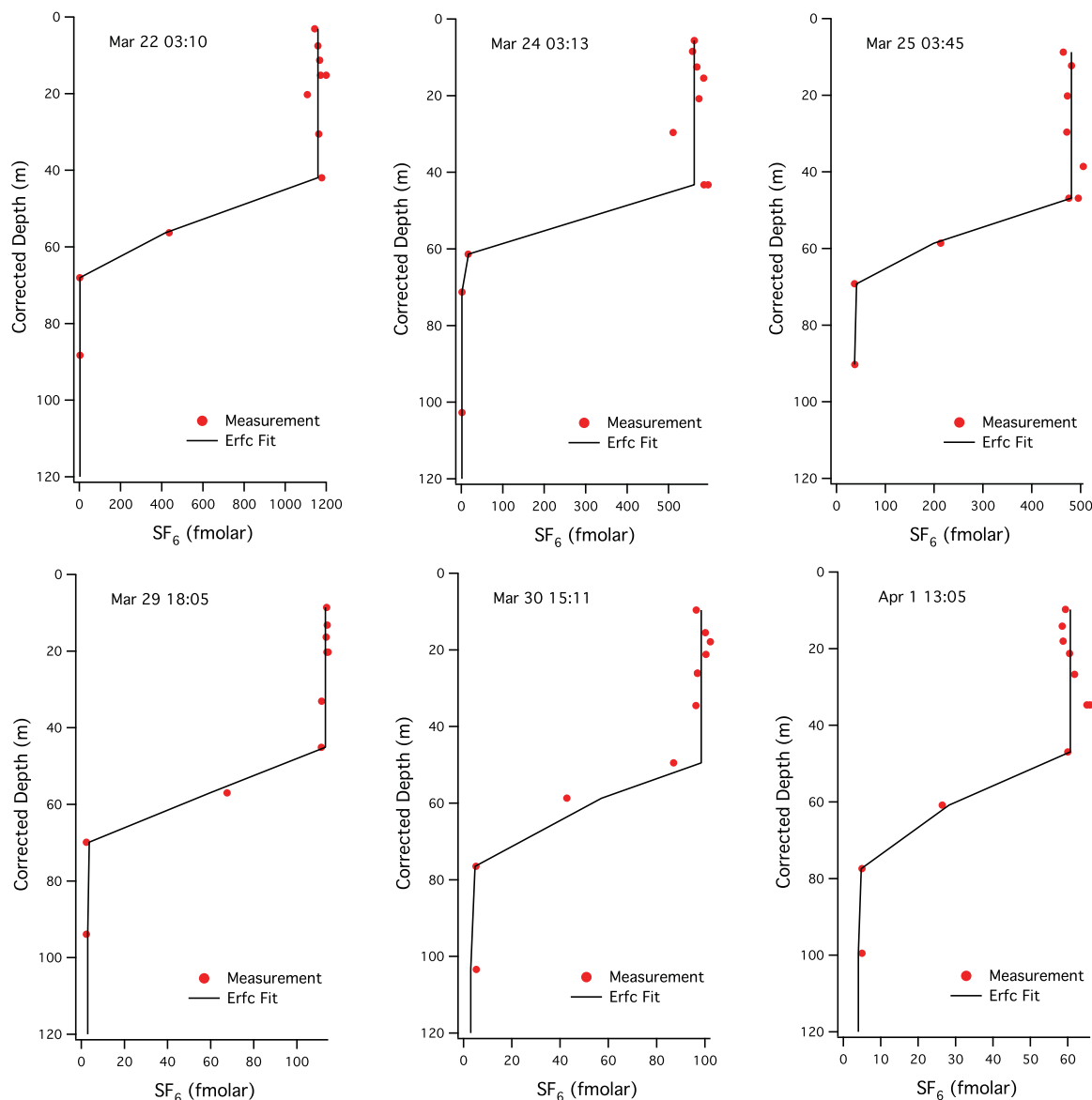
Figure 7. Complementary error function (Erfc) fits of SF_6 profiles for 3 days before and 3 days after the storm using z_{ML} of 53 m and minimized for total error. Depth was corrected for the heaving of internal waves by referencing to the mean depth-density relationship.

coordinates and measured SF_6 concentration relative to the center-of-patch value, with the patch edge operationally defined by the 0.1 contour. For Patch 2, the patch area (A) was approximately 16.5 km^2 by the end of the day of release (21 March), and grew near linearly to 56 km^2 by 25 March. A storm on 26 March sheared the patch into two parts. For the remaining duration of the experiment, the ship mainly followed the larger portion, which spread to 103 km^2 by 2 April. By this time, the 0.1 contour corresponded to ~4 fM, still about twice the background SF_6 concentration.

[27] Following *Bakker et al.* [2005], the horizontal spreading of the patch (fraction per hour) is estimated as $(1/A)(\partial A/\partial t)$, with $\partial A/\partial t$ being the slopes in Figure 9. Spreading rates before and after the shearing of the patch are applied separately to $\langle SF_6 \rangle$ to give the horizontal dilution of SF_6 (H_{SF6}) in units of flux. Over the duration of the

Patch 2, lateral dilution explains ~80% of the SF_6 concentration decrease at patch center.

3.4. Modeled SF_6 Evolution

[28] We examine the robustness of our individual rates above by calculating the implied SF_6 evolution every hour and compare to observations during Patch 2 (Figure 10):

$$\langle SF_6 \rangle_t = \langle SF_6 \rangle_{t-1} - F_{SF6,t-1} + E_{SF6,t-1} - H_{SF6,t-1} \qquad (8)$$

[29] The last three terms on the RHS represented hourly integrated rates since the last time step. We choose 22 March as the starting point, after SF_6 had been thoroughly mixed within the ML. As shown in Figure 10, the implied SF_6 column integrated concentration matches observations fairly well. If we solve for vertical dilution as the residual term in equation (8), budget closure dictates K_z to be less
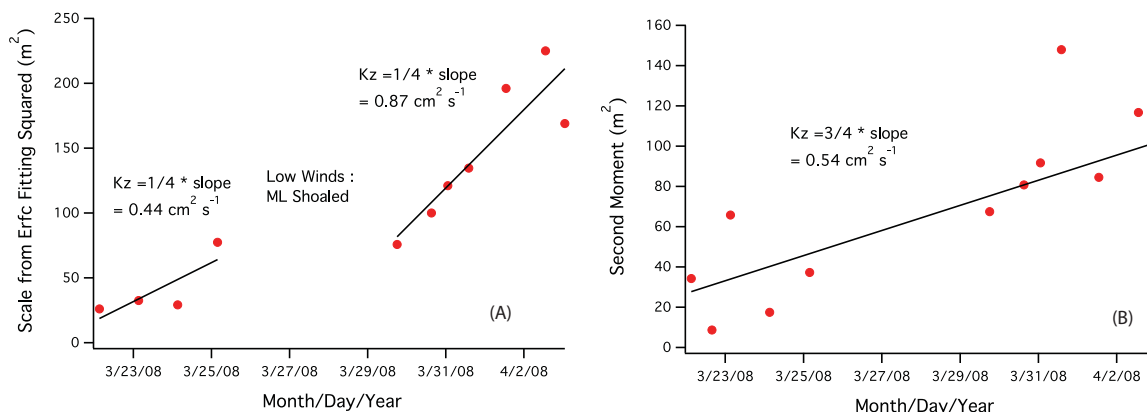
Figure 8. (a) K_z of ~0.4 cm² s⁻¹ and ~0.9 cm² s⁻¹ were separately estimated for before 26 March and after 29 March from the complementary error function fittings of SF₆ vertical profiles; fitting over the entire period of Patch 2 yields 0.6 cm² s⁻¹; (b) K_z of 0.5 cm² s⁻¹ was estimated from Patch 2 based on the evolution of the second moment from the same SF₆ profiles.

than 1.4 cm² s⁻¹, consistent with our estimates from section 3.2 given the uncertainties. In Appendix section A2, we calculate the vertical nutrient fluxes at the base of the ML for Patch 2. The close agreement between the vertical flux and observed time rate of change for silicate serves as another check for K_z. A full SF₆ budget for Patch 1 was not attempted given the short duration and low K_z.

4. DMS Budget

[30] Knowing the physical constraints, we now turn our attention to DMS cycling. In units of flux (e.g., μmoles m⁻² d⁻¹), the DMS budget within the ML may be represented as

$$\frac{\partial \langle DMS \rangle}{\partial t} = -F_{DMS} + E_{DMS} - L_{DMS,photo} + P_{DMS,bio} - L_{DMS,bio} \quad (9)$$

[31] Underway DMS measurements (DMS_0) were averaged to hourly intervals and multiplied by MLD_{SF6} to yield the ML integrated values $\langle DMS \rangle$. The first three terms on the RHS represent the sea-to-air flux, vertical flux, and photochemical loss, and the last two terms on the RHS are biological production and consumption of DMS. Because underway DMS observations do not show a systematic trend between inside and outside the SF₆ patch, horizontal mixing is not considered in the DMS budget.

4.1. Sea-to-Air Flux of DMS

[32] Previous DMS budget studies generally relied on transfer velocity parameterizations as a function of wind speed to estimate the air-sea flux of DMS from bulk concentrations. As shown by *Yang et al.* [2011], even after normalization for diffusivity, DMS transfer velocity (k_{DMS}) is lower than common gas exchange parameterizations derived from sparingly soluble gases [e.g., *Wanninkhof*, 1992; *Nightingale et al.*, 2000] in moderate to high wind speeds. In SO GasEx, we measured the sea-to-air flux of DMS directly with eddy covariance on an hourly basis [*Yang et al.*, 2011]. Because the method required undistorted winds, accurate flux values could only be derived when winds were coming over the bow and when the ship

was not turning rapidly. These conditions were satisfied for approximately half of the cruise. To generate a continuous time series in flux, instead of direct interpolation, we opt for a semiempirical approach:

$$F_{DMS} = k_{DMS}(DMS_0 - \alpha_{DMS} \cdot DMS_{atm}) \quad (10)$$

[33] Here DMS_{atm} is the hourly mean atmospheric concentration observed at 18 m, and α_{DMS} is the dimensionless Ostwald solubility of DMS [*Dacey et al.*, 1984]. k_{DMS} is derived from the in situ transfer velocity versus wind speed relationship. For Patch 2, ventilation to the atmosphere accounted for ~43% of the total physical loss in DMS, and ~24% of the observed decrease in ML concentration after 24 March. For Patch 1, air-sea exchange explains ~45% of the total physical loss in DMS.

4.2. Vertical Mixing of DMS

[34] With low DMS concentration (~0.2 nM) below the pycnocline, vertical mixing depleted $\langle DMS \rangle$. The vertical
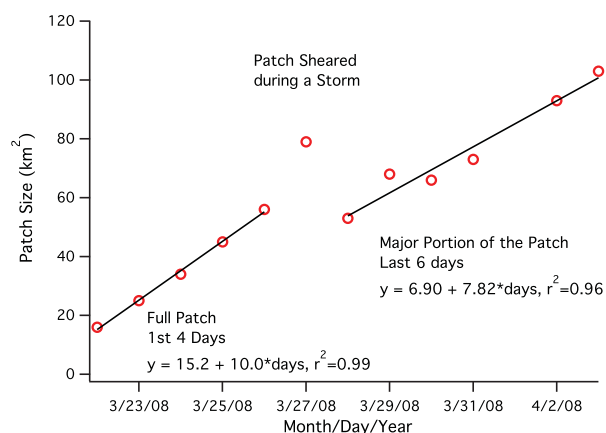

Figure 9. Horizontal dilution estimated from the linear increase in tracer patch area, which was determined from daily contours and corrected for surface current. The edge of the patch is operationally defined as where the SF₆ concentration was 10% of the concentration in the center of the patch.
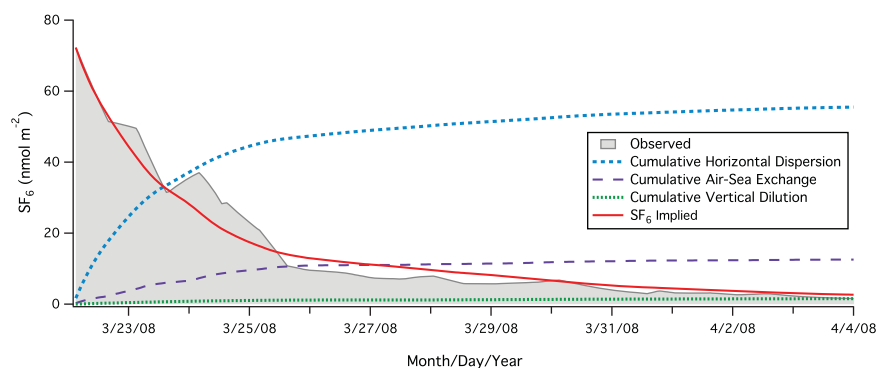
Figure 10. The implied SF_6 evolution agrees well with observed time rate of change in ML SF_6 concentration at patch center for Patch 2. Horizontal dilution contributes by far the most to the decrease in SF_6 concentration, followed by sea-to-air transfer and vertical mixing.

flux of DMS (E_{DMS}) at the base of the ML is calculated analogously to equation (7) using concentrations from the CTD casts. For Patch 2, with K_z of $0.4{\sim}0.9$ cm^2 s^{-1}, vertical mixing accounted for $\sim$10% of the total physical loss and $\sim$6% of the observed decrease in $\langle DMS \rangle$ after 24 March. For Patch 1, with a lower K_z of 0.3 cm^2 s^{-1}, vertical mixing accounted for $\sim$6% of the total physical loss. The DMS:DMSP ratios within and below the ML were fairly similar (Figure 3). Thus, vertical mixing should not have significantly altered the DMS:DMSP ratio.

4.3. Photochemical Loss of DMS

[35] The photochemically mediated destruction of DMS depends on the underwater light field and concentrations of light absorbing compounds (photosensitizers), as DMS itself does not absorb radiation at wavelengths over 260 nm [*Brimblecombe and Shooter*, 1986]. A number of studies have found nitrate and CDOM to be the two most important photosensitizers for DMS photochemistry [*Toole et al.*, 2004; *Bouillon and Miller*, 2004], with the bulk of the reaction ($\sim$65%) initiated by UVA light (320$\sim$400 nm).

[36] Following *Toole et al.* [2003], we estimate the surface photochemical loss rate (L_0) at solar noon within the wavelength (λ) range of 280$\sim$420 nm:

$$L_0 = \int_{280\ nm}^{420\ nm} a_{CDOM} E_0 \Phi d\lambda \qquad (11)$$

[37] Here a_{CDOM} is the measured absorption of CDOM in units of m^{-1} by a multispectral absorption-attenuation sensor (Wetlabs-acs, 250$\sim$700 nm) fitted with a 0.22 μm filter [*Del Castillo and Miller*, 2011]. At 300 nm, CDOM absorption in Patch 1 and 2 were on the order of 0.3 and 0.4 m^{-1}, respectively [*Del Castillo and Miller*, 2011]. We approximate the spectral scalar irradiance at the surface (E_0) to be 1.2 times the spectral downwelling irradiance (E_d), in units of moles of photons m^{-2} s^{-1} nm^{-1} [*Toole et al.*, 2003]. Lacking in situ UV measurements, we use E_d from the NCAR Tropospheric Ultraviolet and Visible (TUV) Radiation Model (http://cprm.acd/ucar.edu/Models/TUV/) at the location and time of SO GasEx at solar noon. Φ in equation (11) represents the apparent quantum yield of DMS (moles of DMS photolyzed per moles of photons absorbed by CDOM) normalized to the

DMS concentration, in units of m^3 moles of photons^{-1}. *Bouillon and Miller* [2004] reported a linear dependence between Φ at 330 nm and nitrate concentration in μM: $0.15[NO_3]+0.41$. Following their work, spectral Φ is estimated as: $\Phi_\lambda = \Phi_{330} e^{-0.036(\lambda-330)}$. At a Patch 2 mean nitrate concentration of 15 μM and integrating over the wavelengths considered, the surface photochemical loss rate is on the order of 0.1 h^{-1} at solar noon for Patch 2.

[38] In comparison, *Toole et al.* [2004] measured a L_0 of $0.16{\sim}0.23$ h^{-1} in the Ross Sea in November from shipboard incubation with ^{35}S-DMS. CDOM absorption at 300 nm was $0.24{\sim}0.31$ m^{-1}, while the nitrate concentration was $\sim$29 μM in their experiment. *Toole et al.* [2004] also reported a near-linear dependence of L_0 on nitrate concentration: $0.0032[NO_3]+0.107$, which at a nitrate concentration of 15 μM amounts to 0.16 h^{-1}. Given the differences in time, location, and waters between the Ross Sea and near South Georgia Island, the similarity between the two L_0 estimates above is reassuring.

[39] Because the intensity of UVR decreases quickly with depth, photochemical loss of DMS depends strongly on MLD. Assuming exponential decay in light intensity, we estimate the DMS photochemistry rate at depth (z) as $L_z = L_0 e^{-K_d \cdot z}$. The UV diffuse attenuation coefficient (K_d) was determined using the global in-water model of *Smyth* [2011]. The model uses water leaving reflectance data from the Sea viewing Wide Field-of-view Sensor (SeaWiFS, http://oceancolor.gsfc.nasa.gov) to determine Inherent Optical Properties in visible wavelengths [*Smyth et al.*, 2006] between 1998 and 2009. From this a monthly climatology K_d (UV) was determined [*Smyth*, 2011] and the data from the month of March in the region of interest extracted (T. Smyth, personal communication, 2011). At an average of 0.17 m^{-1} between 280 and 420 nm, K_d in SO GasEx is twice the value reported by *Toole et al.* [2004], consistent with the higher CDOM concentration observed near South Georgia Island. Since the DMS concentration is largely constant with depth within the ML, we approximate the time-dependent photochemical loss of DMS as

$$L_{DMS,photo} = DMS_0 \frac{SW}{SW_{noon}} \int L_z \cdot dz \qquad (12)$$

[40] Here SW is the incoming shortwave irradiance at a given time; SW_{noon} is the irradiance at solar noon, which

averaged ~500 W m^{-2} during Patch 2. Given the number of assumptions and simplifications, uncertainties in $L_{DMS,photo}$ are likely significant (at least 50%). As such, for Patch 2 photochemistry accounted for ~47% of the total physical loss in DMS and a quarter of the observed concentration decrease after 24 March. For Patch 1, photochemistry accounted for 49% the total physical loss of DMS.

4.4. Biological Production and Consumption of DMS

[41] The biological production and consumption of DMS in equation (9) were not measured during SO GasEx. Direct quantification of total DMS production is challenging. Incubation experiments involving the addition of radio-labeled DMSP$_d$ or inhibitors such as dimethyldisulphide (DMDS) usually only account for bacterial DMS production, but not direct production by algae or contributions from grazing or viral lysis. *Bailey et al.* [2008] surveyed previous gross DMS production measurements and found them to span over three orders of magnitude. However, when normalized by the concentration of total DMSP, the range in DMS production rates narrows to one order of magnitude in different oceanic environments: 0.05~0.7 nM DMS (nM DMSP)$^{-1}$ d^{-1}. *Hermann et al.* [2011] used diagnostic modeling to estimate DMS production in the coastal waters of Antarctica. Combining with data from *Bailey et al.* [2008], *Hermann et al.* [2011] argued for a universal DMS production rate of 0.06 ± 0.01 nM DMS (nM DMSP)$^{-1}$ d^{-1}. Assuming the gross production rate of DMS is depth-independent within the ML, we initially approximate $P_{DMS,bio}$ (in units of µmoles m^{-2} d^{-1}) as 0.06⟨DMSP⟩, where ⟨DMSP⟩ is the in situ concentration of DMSP integrated over the ML. For Patch 2, ~20 nM of DMSP implies a $P_{DMS,bio}$ of ~70 µmoles m^{-2} d^{-1}, or ~1.2 nM d^{-1}. For Patch 1, because of the greater DMSP concentration, $P_{DMS,bio}$ is expected to be about three times higher. These rates would be about an order of magnitude higher than the physical losses of DMS.

[42] Observations of biological consumption of DMS in the Southern Ocean are relatively scarce. From three separate transects in November and December in the New Zealand Sector of the Southern Ocean, *Kiene et al.* [2007] reported fairly low rate constants (k_{bc}) in open water, usually on the order of ~0.2 d^{-1}. From the Ross Sea, Antarctica, *del Valle et al.* [2009] measured k_{bc} with a range of typically 0.1~1.0 d^{-1}; higher rates were observed in the summer (0.2~1.0 d^{-1}) than in the spring (0.05~0.21 d^{-1}). For simplicity, we assume the biological consumption rate of DMS to be a first-order process and k_{bc} to be invariant in our model.

4.5. Modeled DMS Evolution

[43] From equation (9), the hourly evolution of DMS in the ML is modeled as

$$\langle DMS \rangle_t = \langle DMS \rangle_{t-1} - F_{DMS,t-1} + E_{DMS,t-1} - L_{DMS,photo,t-1} + P_{DMS,bio,t-1} - L_{DMS,bio,t-1} \qquad (13)$$

[44] The last five terms on the RHS represent time-integrated rates since the previous hour, with $L_{DMS,bio,t-1} = k_{bc} \langle DMS \rangle_{t-1}$. The modeled DMS evolution in the two tracer patches are shown in Figures 11 and 12, with individual rates specified in the bottom plots.
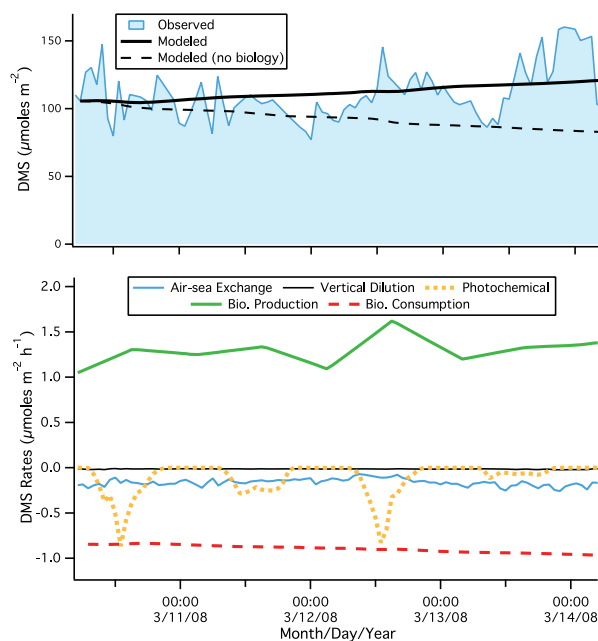

Figure 11. (top) Observed and modeled DMS evolution with and without biology from Patch 1; (bottom) individual rates, with a positive/negative sign indicating a source/sink for ML DMS. The observed time rate of change was 6.6 µmoles m^{-2} d^{-1}, while the total physical loss was about −5.8 µmoles m^{-2} d^{-1}, implying a net biological DMS production of 12.4 µmoles m^{-2} d^{-1}. Total biological DMS production was assumed to be (in units of µmoles m^{-2} d^{-1}) 0.01⟨DMSP⟩, while biological DMS consumption was modeled as a first-order loss required for budget balance (k_{bc} = 0.2 d^{-1}).

[45] Also shown are the implied DMS concentrations in the absence of any biological processes. For Patch 1, the observed rate of change over time was 6.6 µmoles m^{-2} d^{-1}, while the total physical loss was about −5.8 µmoles m^{-2} d^{-1}, implying a net biological change of ~12.4 µmoles m^{-2} d^{-1}. For Patch 2, the initial increase in DMS concentration over the first three days was 11.0 µmoles m^{-2} d^{-1}; the corresponding total physical loss in DMS was at −14.7 µmoles m^{-2} d^{-1}, yielding a rapid net biological production of 25.7 µmoles m^{-2} d^{-1}. Physical losses can account for about half of the observed rate of decrease in DMS concentration since 25 March, which was −11.3 µmoles m^{-2} d^{-1}; this implies a net biological change of −5.3 µmoles m^{-2} d^{-1} during this period. The individual rates are summarized in Table 1.

[46] Are the biological DMS production and consumption rates we initially assumed reasonable? For Patch 1, a value of 1.6 d^{-1} for k_{bc} is needed to balance the production of (0.06⟨DMSP⟩) µmoles m^{-2} d^{-1}, which would be significantly higher than previously measured rate constants for biological DMS turnover in the Southern Ocean [*Kiene et al.*, 2007; *del Valle et al.*, 2009]. To balance a more likely k_{bc} value of 0.2 d^{-1}, the biological production term would need to be reduced by a factor of six (i.e., 0.01⟨DMSP⟩), which is the scenario shown in Figure 11. Using k_{bc} = 0.2 d^{-1} and a production rate of 0.01⟨DMSP⟩
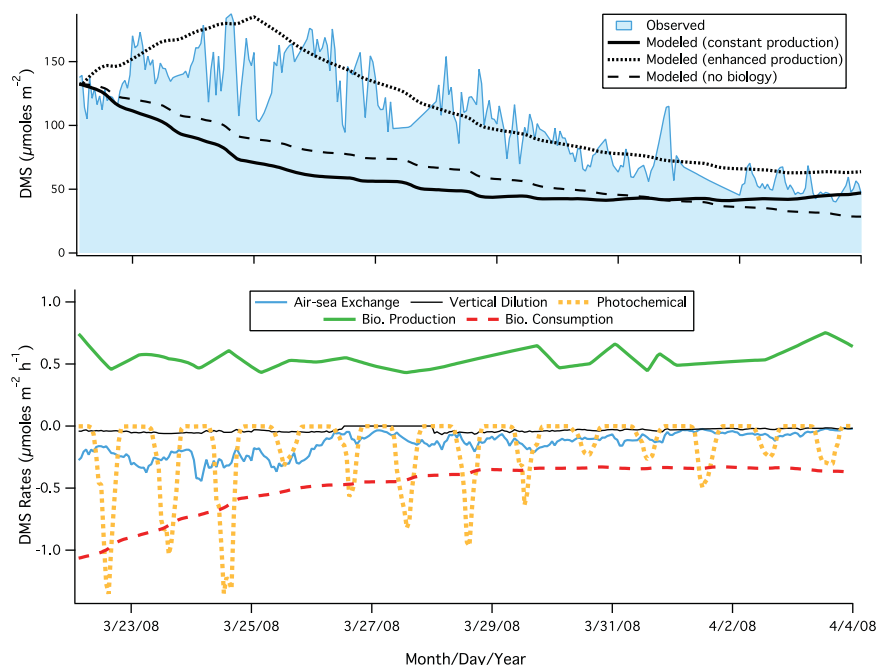
Figure 12. (top) Observed and modeled DMS evolution from Patch 2; (bottom) individual rates for the case of constant production. Total physical loss can account for about half of the decrease in DMS concentration after 24 March (-11.3 μmoles m^{-2}), implying a net biological production of -5.3 μmoles m^{-2} d^{-1} during this period. Using a consumption rate constant of 0.2 d^{-1}, modeled DMS concentration with a production of $0.01\langle DMSP\rangle$ is lower than observed. The initial increase in DMS concentration can be simulated by increasing DMS production in the first 3 days by a factor of five.

for Patch 2, modeled DMS evolution is lower than observed (Figure 12). In fact, with a constant (i.e., proportional) DMS production rate from DMSP, it is not possible to replicate the increase in DMS concentration over the first few days of Patch 2 regardless of the k_{bc} chosen. If instead we allow the DMS production rate to be a factor of five higher for the first 3 days of Patch 2, then the observed DMS evolution appears to be fairly well simulated by the model. It seems that the actual biological production rate of DMS was variable and not always proportional to DMSP concentration.

[47] At a modest k_{bc} of 0.2 d^{-1}, biological consumption still accounts for ~80% of the total DMS loss. The dominant role of biological turnover in DMS cycling for SO GasEx would be consistent with findings from *Kiene and Bates* [1990], *Bates et al.* [1994], *del Valle et al.* [2009], and so on. In contrast to measurements from *Toole et al.* [2004] in the Antarctic summer, photochemistry rate during SO GasEx was modest likely because the experiment took place in the austral fall, with shortening daylight. Counterintuitive in some ways, air-sea DMS flux during SO GasEx was the lowest among the five open ocean cruises summarized by *Yang et al.* [2011]. Despite strong winds, high gas solubility as a result of low temperature significantly limits the oceanic emission. Last, vertical mixing at the base of the pycnocline only alters the ML DMS concentration slightly in this case. However, as shown below, the accompanying changes in nutrients and biological composition might have influenced the DMS budget significantly.

5. Discussions

5.1. Biological Community Composition and Net Community Production

[48] From *Lance et al.* [2012], the main diagnostic pigments for phytoplankton during SO GasEx were fucoxanthin (FUCO; e.g., diatoms, which produce low amounts of DMSP) and 19′-hexanoyloxyfucoxanthin (HEXA, e.g., prymnesiophytes, which produce high amounts of DMSP). For Patch 1, FUCO decreased slightly while HEXA

Table 1. DMS(P) Concentrations, Ratios, and Rates[a]

	Patch 1	Patch 2	Patch 2
	10~14 Mar	22~24 Mar	25 Mar~4 Apr
<DMS>	111	142	93
<DMSP>	3266	1472	1263
DMS/DMSP	0.03	0.10	0.07
DMSP/Chl$a$	74	34	45
d<DMS>/dt	6.6 ± 1.6	11.0 ± 2.4	-11.3 ± 0.4
Air-Sea Exchange	-2.6 ± 0.3	-6.2 ± 0.6	-2.6 ± 0.3
Photochemistry	-2.8 ± 1.4	-7.4 ± 3.7	-2.7 ± 1.4
Vertical Mixing	-0.4 ± 0.4	-1.1 ± 0.6	-0.7 ± 0.2
Total Physical Loss	-5.8 ± 1.5	-14.7 ± 3.8	-6.0 ± 1.4
Net Biological Change	12.4 ± 2.2	25.7 ± 4.5	-5.3 ± 1.5

[a]Mean <ML Concentrations> in μmoles m^{-2}. Rates in μmoles m^{-2} d^{-1}. Positive (minus) sign denotes increase (decrease) in ML concentrations. 10% and 50% uncertainties approximated for air-sea exchange and photochemistry. Other uncertainties propagated from error. DMS/DMSP dimensionless. DMSP/Chla in nmol μg^{-1}.

increased, causing the HEXA:FUCO ratio to increase from 0.75 to 0.90. Based on O_2/Ar measurements [*Hamme et al.*, 2012], the biological community was net autotrophic for Patch 1. At about 17 and 1.2 μM, respectively, nitrate and phosphate concentrations were relatively high and stable during Patch 1.

[49] Patch 2 exhibited at least two biological phases. For the first few days, chlorophyll mass in the ML was dominated by a small diatom bloom (HEXA:FUCO of 0.3∼0.4), even though the O_2/Ar ratio implied net heterotrophy. Over the following 3∼5 days, the concentration of FUCO dropped by threefold, while the concentration of HEXA remained largely unchanged, resulting in an increase in the HEXA:FUCO ratio to ∼0.8. *Lance et al.* [2012] attributed the decrease in FUCO in this phase to preferential consumption of diatoms by grazers, in accord with enhanced ammonium concentrations (mean of 2.2 μM for Patch 2, compared to 1.1 μM for Patch 1). The f-ratio (nitrate based production/primary production) was also lower in Patch 2 (0.15) compared to Patch 1 (0.24), indicating greater regenerated production during the second patch. Toward the end of Patch 2, both HEXA and FUCO increased slightly, while O_2/Ar measurements suggested that the system shifted to slightly autotrophic. Over the 2 weeks of Patch 2, the ML concentrations of nitrate and phosphate increased at rates of 8.3 and 0.75 mmol m^{-2} d^{-1}, respectively, partly due to vertical mixing (Appendix section A2; see figures from *Lance et al.* [2012]). At these concentrations, nitrate and phosphate were not directly limiting the growth of phytoplankton. *Lance et al.* [2012] postulated that the biology might be controlled by the availability micronutrients (e.g., iron), which could be supplied by vertical as well as horizontal mixing. DMS dynamics during these two patches were likely influenced by both the phytoplankton community composition (indicated by the DMSP:Chl*a* ratio), as well as bacterial activity (somewhat reflected in the DMS:DMSP ratio), as discussed below.

5.2. DMSP Utilization and DMS Production

[50] *Kiene et al.* [2000] proposed that the tendency for DMSP to be cleaved or demethylated is related to nutrient availability. While the cleavage of DMSP yields carbon and energy, the demethylation pathway provides bacteria with both carbon and sulfur. Under a high nutrient condition that is favorable for growth (e.g., Patch 1 and end of Patch 2), the demand for sulfur, necessary for bacterial protein synthesis, is high; this might lead to mostly demethylation and little cleavage (i.e., limited DMS production). Also, intracellular DMSP in phytoplankton is physically separated from the enzyme capable of catalyzing the DMSP cleavage reaction, implying that healthy algal populations produce little DMS [*Stefels and van Boekel*, 1993]. This is likely the reason why increasing HEXA:FUCO ratio during the latter part of Patch 2 did not lead to increasing DMS:DMSP. Similarly, for the net autotrophic Patch 1, despite high DMSP concentration, bacterial production of DMS was likely limited, as inferred from the low DMS:DMSP ratio.

[51] In contrast, high DMS production is often found under conditions of stress (e.g., nutrient depletion), which might reflect a greater need for energy and less potential for growth (more cleavage of DMSP), as well as during
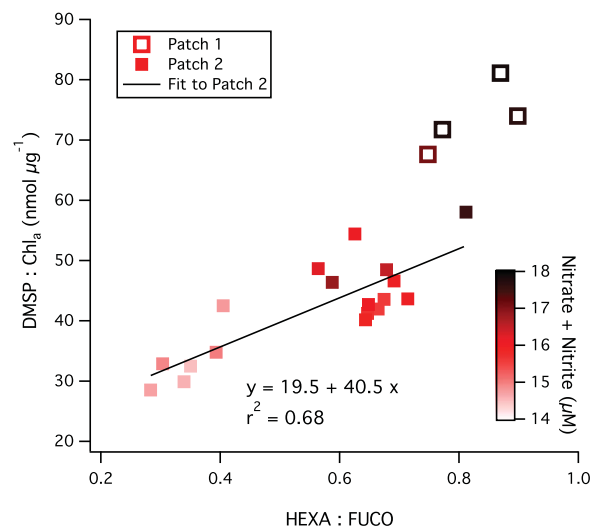

Figure 13. Relationship between DMSP:Chla ratio and HEXA:FUCO, color-coded by concentrations of DIN (nitrate + nitrite). The positive correlation between the two ratios for Patch 2 ($r^2 = 0.68$) is consistent with the higher intracellular DMSP concentration in prymnesiophytes than in diatoms. A higher HEXA:FUCO ratio also coincided with greater DIN concentration, possibly related to the algal succession as a result of changing nutrient supply.

grazing. The initial increase in DMS concentration during Patch 2 was probably related to the short diatom bloom (but overall net heterotrophy). Even though diatoms are less prolific producers of DMSP than prymnesiophytes, preferential grazing of diatoms possibly increased the release of DMSP$_d$, which was quickly converted to DMS by bacteria. After the diatom bloom ceased, the decrease in DMS concentration for the latter stage of Patch 2 was possibly due to reduced DMS production by bacteria (less available DMSP$_d$). We note that given the high concentrations of nitrate and phosphate during SO GasEx, direct limitation caused by these macronutrients was probably unlikely.

[52] The scaling approach of predicting DMS production from DMSP concentration [*Hermann et al.*, 2011] might be useful on a large scale, but is likely too simplistic to predict short-term changes. A better model needs to differentiate between algal and bacterial DMS productions and incorporate grazing by zooplankton [e.g., *Archer et al.*, 2004; *Polimene et al.*, 2012]. While trends in DMS concentration could also be explained by changes in microbial consumption, this seems less likely as DMS degradation involves specific bacterial community that are not expected to be highly variable within a timescale of a few days [e.g., *Zubkov et al.*, 2002a, 2002b].

5.3. DMSP:Chla and DMS:DMSP Ratios as Biological Indicators

[53] Figure 13 shows a positive correlation ($r^2 = 0.68$) between DMSP:Chl*a* (in nmol μg^{-1}) and HEXA:FUCO for Patch 2, color-coded by concentrations of dissolved inorganic nitrogen (DIN = nitrate + nitrite). These ratios from Patch 1 also follow the same general trend, consistent with the findings that prymnesiophytes have higher
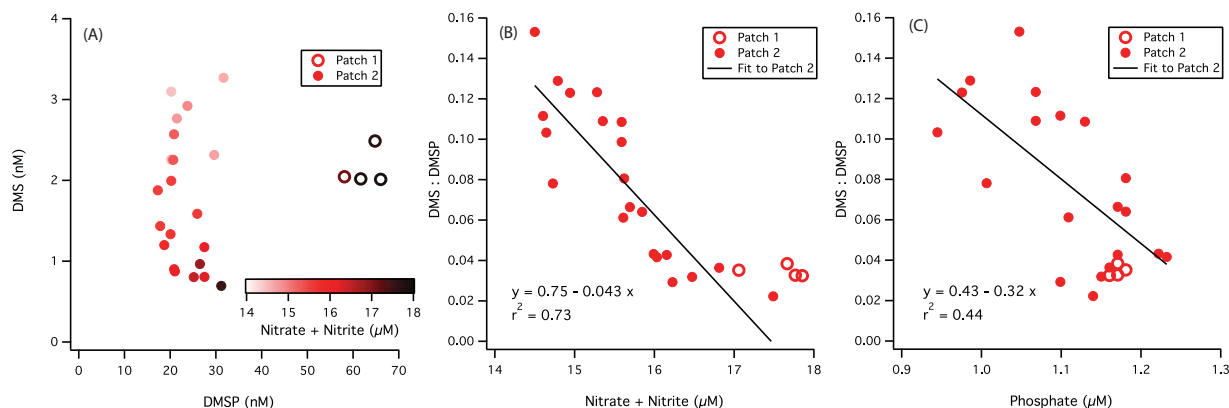
Figure 14. (a) DMS versus DMSP near the surface, color-coded by DIN concentration and (b) DMS:DMSP ratio versus DIN concentration; DMS:DMSP ratio versus phosphate concentration. The steeper slope and greater r^2 of DMS:DMSP with DIN versus with phosphate might be in part due to nitrate induced photochemical loss of DMS. Other possible reasons for the negative relationships include changes in bacterial utilization of DMSP as well as phytoplankton community composition and production.

intracellular DMSP content than diatoms. This demonstrates the potential usefulness of the DMSP:Chl$a$ ratio as an indicator for phytoplankton community change, possibly in response to nutrient availability.

[54] Correspondence between DMSP and DMS concentration, however, was not obvious. A plot of these two variables (Figure 14a) clearly shows two distinct groupings. As indicated by color-coding, at the same DMSP concentration, decreasing DMS concentration was observed with increasing DIN. This is illustrated more clearly in Figure 14b, where the DMS:DMSP ratio appears to be negatively correlated with DIN, with a r^2 of 0.73 for Patch 2. A negative relationship is also found between DMS:DMSP with phosphate concentration, but with a weaker correlation (r^2 of 0.44; Figure 14c). Such negative correlations of DMS:DMSP with DIN and phosphate have been reported from a diatom-dominated bloom in the Ross Sea by *Smith* [2011]. There are likely multiple reasons for these negative relationships. If we divide the slope between DMS:DMSP versus phosphate (-0.32) by the mean N:P ratio of 14 for Patch 2, the result (-0.023) is about half of the slope between DMS:DMSP versus DIN (-0.043). The steeper slope and greater r^2 between DMS:DMSP and DIN might be partly explained by nitrate-induced photochemical destruction of DMS. In addition, increasing nutrient concentrations could have led to greater bacterial sulfur demand (such that more DMSP could have been demethylated instead of cleaved to DMS) and also coincided with shifts in the biological community composition and production. Overall, the DMS:DMSP ratio appears to be lower during net autotrophy than during net heterotrophy. The decoupling between DMS and DMSP suggests important roles for microbially mediated DMS production and zooplankton grazing.

6. Conclusions

[55] In a Lagrangian study in the Southern Ocean in the austral fall, turbulent mixing rates determined from deliberate tracer releases and direct measurements of gas exchange constrain the physical environment, allowing us to examine the net biological changes in DMS following two water patches. Vertical mixing at the base of the ML accounted for only a small of loss of SF_6 from the ML ($\sim$2% for Patch 2); most of the SF_6 was removed from patch center via horizontal spreading (80%) and sea-to-air emission (18%). For DMS, among physical losses, contributions from photochemistry, sea-to-air emissions, and vertical mixing were $\sim$49%, 45%, and $\sim$6%, respectively, for Patch 1; they were $\sim$47%, $\sim$43%, and $\sim$10%, respectively, for Patch 2.

[56] Biological production and consumption (inferred) appeared to dominate the DMS budget. The observed trends in DMS concentration were thus the results of small differences between two large, opposing terms, such that minor changes in the biological community composition and production can potentially have a large impact on the DMS standing stock on timescales of days. A constant DMS production rate as a function of DMSP concentration cannot explain the observed DMS evolution during Patch 2. This suggests that DMS production was likely variable and dependent on both plankton and bacterial processes. The DMSP:Chl$a$ ratio appears to be a useful indicator for a phytoplankton assemblage dominated by diatoms and prymnesiophytes. The DMS:DMSP ratio was consistently low during periods of high nutrient supply and greater autotrophy.

Appendix A

[57] Figure A1 shows the depth versus density relationship for Patch 2, color-coded by time. The black dots indicate the mean density-depth relationship. Figure A2 shows the evolution of the ML, represented here by the density-corrected depth where SF_6 concentration was half of the ML mean.

A1. Vertical Diffusivity Estimates

[58] The complementary error function method assumes that changes in the shapes of SF_6 profiles over time are driven only by vertical mixing, which is described by a
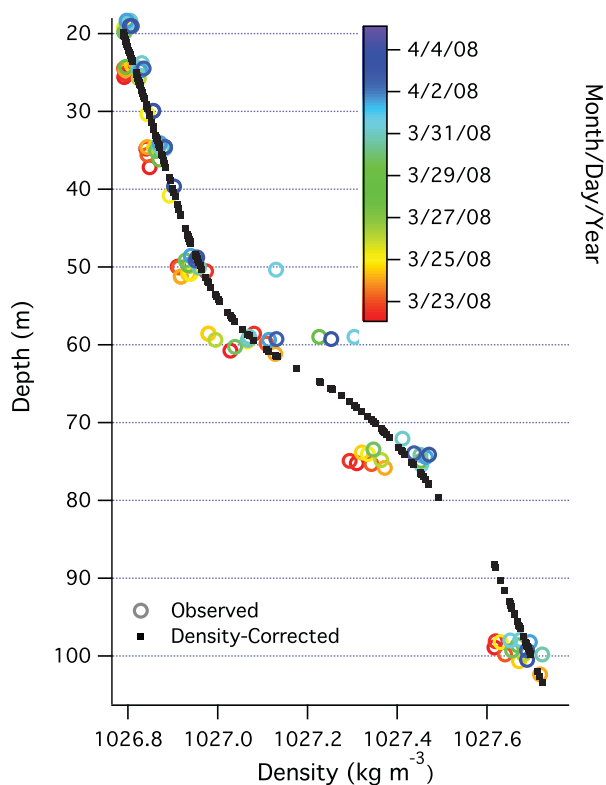
Figure A1. Large scatter in density at a given depth near the pycnocline is partly due to internal waves, which we remove by referencing to the mean depth versus density relationship (black dots). The isopycnals (e.g., 1027 kg m^{-3}) appeared to have shoaled over time at an approximate rate of 0.5 m d^{-1}.

constant K_z within the pycnocline during the time interval considered. Fitting should be insensitive to changes in concentration due to lateral dispersal provided that vertical shear in the horizontal currents was minimal within the ML. Estimated K_z depends on the target MLD (Z_{ML}). We allow Z_{ML} to vary from 19 to 64 m and σ to vary from 1 to 39 m in equation (4). The final value of σ for a given profile is determined by minimizing the square of the difference between the log of the fit and the log of the measured concentration. We can visualize the change in SF$_6$ profiles by plotting contours representing the error (the square of the difference between the logs) in the space of σ versus Z_{ML} (Figure A3). With time, the location of minimum error moves upward due to vertical mixing. At a lower Z_{ML}, the calculated σ of minimum error increases, which leads to a larger K_z. Decreasing/increasing Z_{ML} by 1 m results in ~10% increase/decrease in computed K_z. The density correction on depth is essential here due to the large variability in MLD caused by internal waves. Repeating the same fittings above with uncorrected depth results in σ^2 too scattered for a statistically meaningful regression.

[59] Using the same SF$_6$ vertical profiles, an alternate method for estimating K_z involves evaluating the evolution of the second moment (M_2) of SF$_6$ within the pycnocline, which is detailed by *Law et al.* [1998, 2001, 2003]. To calculate M_2, we linearly interpolate SF$_6$ profiles to 2.5 m depth intervals from 52.5 m to 100 m and use the concen-

tration between 95 and 100 m as the background value. Following *Law et al.* [2003], K_z is estimated as $3/4$ dM_2/dt to be approximately 0.5 cm^2 s^{-1} over the entire duration of Patch 2 (r^2 of linear regression of 0.46, Figure 8b). As the calculated M_2 depends strongly on the low concentration "tail" of SF$_6$ at deeper depth, this method is less robust than the complementary error function fit. Nevertheless, the fact that both methods lead to similar K_z estimates over the duration of Patch 2 is reassuring.

[60] We briefly examine other measurements of K_z at the base of the ML from SF$_6$, profiles in the Southern Ocean. In the Antarctic Circumpolar Current, *Law et al.* [2003] determined a K_z of 0.11 ± 0.2 cm^2 s^{-1}. From a cyclonic eddy north of the Antarctic Polar Front, *Goldson* [2004] estimated a K_z of 0.54 ± 0.8 cm^2 s^{-1}. Our results are within uncertainties of those previous estimates. However, the K_z we estimated might not be purely diapycnal because of rapid changes in the MLD; thus errors in our K_z values are likely larger than what are quoted in section 3.2. *Law et al.* [2001] stated that deepening of the isopycnals due to entrainment would dilute the SF$_6$ concentration above the target isopycnal (or Z_{ML}). Thus by using the mean density-corrected depth, the erfc fitting could underestimate K_z. Overall, our estimate may be considered an effective diffusivity that fit the observed tracer evolution, while encompassing nondiapycnal processes.

[61] As described by *Ho et al.* [2011a], vertical diffusivity during SO GasEx had been estimated from a one-dimensional (1-D) Generalized Ocean Turbulence Model (GOTM) based on transport of heat, salt, and momentum. At the base of the GOTM mixed layer (as defined by density), the modeled K_z varies over five orders of magnitude, with a mean of 4 cm^2 s^{-1} and median of 0.2 cm^2 s^{-1} over the duration of Patch 2. The mean greatly exceeds the median here because bulk of the vertical mixing is caused by few episodic turbulent events [*Gregg*, 1987]. Our estimated K_z from SF$_6$ profiles is lower than the GOTM mean but higher than the median. Part of this discrepancy may be related to the fact that MLD$_{SF6}$ was usually deeper than MLDρ, while K_z likely decreases with depth near the ML base. Unfortunately, this cannot be tested directly in
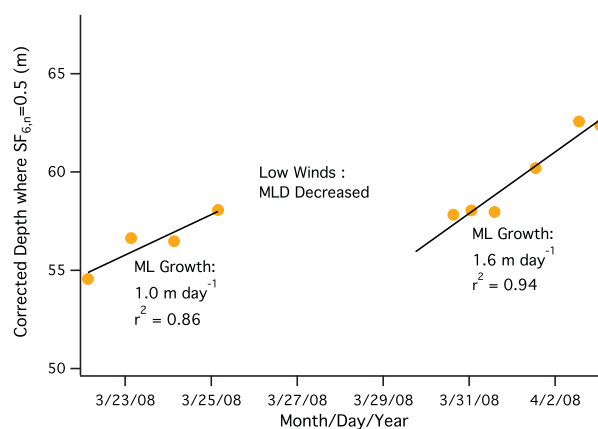

Figure A2. Change of the corrected depth where the depth-normalized SF$_6$ concentration was half of the ML mean. The mixed layer deepened at a rate of 1.0 and 1.6 m d^{-1} before and after the storm.
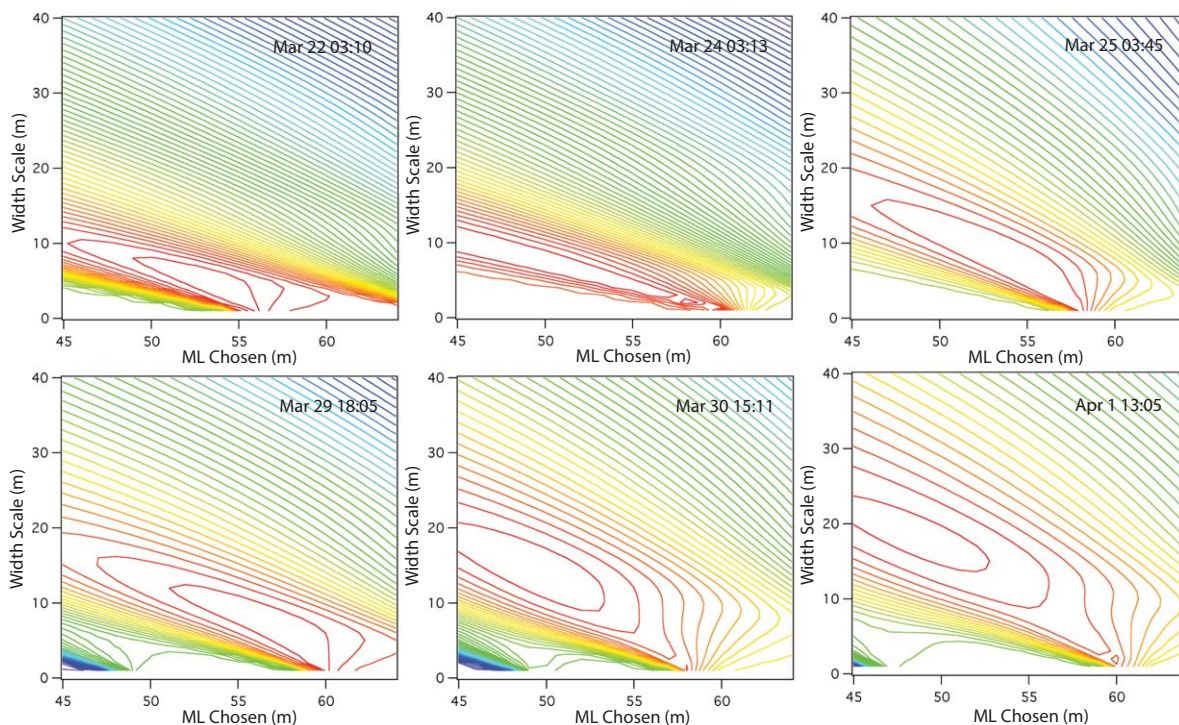
Figure A3. Total error (sum of the square of difference between logs) from the complementary error function fittings of SF_6 Profiles for 3 days before and 3 days after the storm, presented as contours in coordinates of width scale versus ML chosen. The red contours indicate regions of minimum total error, which are seen to progress upward with time. For a fixed target ML (Z_{ML}), a linear trend of the square of the width scale (of least error) versus time is proportional to the vertical diffusivity at the base of the mixed layer.

GOTM because the model does not have a realistic internal wavefield and thus underestimates vertical mixing below the mixed layer.

[62] We can also compare the vertical velocity associated with K_z to the observed ML deepening. For Patch 2, at K_z of 0.4 and 0.9 cm^2 s^{-1} before and after the storm, $K_z/\Delta z$ is on the order of 0.5~0.8 m d^{-1}, lower than the entrainment velocity estimated from the deepening of the density-corrected MLD (1.0~1.6 m d^{-1}). This suggests that changes in the MLD in Patch 2 were not entirely due to vertical mixing, consistent with the apparent shoaling of the isopycnals inferred from Figure 6.

A2. Vertical Nutrient Supply

[63] To test for the robustness of our K_z estimate and to explore what was causing the biological community change, we calculate the supply of nutrients from below the ML and compare to their observed time rate of change during Patch 2. Time series and vertical profiles of macronutrients were shown by *Lance et al.* [2012]. Taking the concentration jump as the difference between the base of the pycnocline and at ~75 m, at K_z = 0.9 cm^2 s^{-1} the vertical fluxes of silicate, nitrate, phosphate, and ammonium averaged 5.7, 3.8, 0.31, and 0.43 mmol m^{-2} d^{-1}. In comparison, temporal trends in the ML integrated nutrient concentrations correspond to increases in silicate, nitrate, and phosphate of 5.6, 8.3, and 0.75 mmol m^{-2} d^{-1}. Ammonium concentration increased at 0.92 mmol m^{-2} d^{-1} but was

more variable, likely reflecting rapid production (e.g., from grazing) and biological uptake. Aside from a brief diatom bloom at the beginning of Patch 2, the consumption of silicate should be limited. Thus, the close agreement between vertical flux of silicate and its observed increase suggests that our K_z value is appropriate. However, the vertical fluxes of nitrate and phosphate appear to be only half of the observed increases. The residual increases in nutrient concentrations are unlikely to be explained by remineralization, which takes place mostly below the ML and above 1000 m [e.g., *Arístegui et al.*, 2002]. Even if we assume all of the decrease in particulate organic carbon concentration during Patch 2 was due to remineralization, the corresponding release of nitrate and phosphate only amount to small fractions of their observed time rates of change. Biological consumption of nitrate and phosphate also did not appear to have a major effect on the observed time rate of change. From ^{15}N incubation [*Lance et al.*, 2012], the new production during Patch 2 ranged 1.9~7.1 mmol C m^{-2} d^{-1}. At Redfield ratios, nitrate and phosphate consumption rates would be only 0.3~1.1 mmol m^{-2} d^{-1} and 0.02~0.07 mmol m^{-2} d^{-1}, respectively.

[64] A more likely explanation for the "missing source" of nutrients is horizontal mixing with water from the south. In GOTM, local surface forcing appears insufficient to explain the cooling and increasing densities during Patch 2 [*Ho et al.*, 2011a]. The authors postulated that colder and saltier water was likely mixed into the patch from the south. Higher nitrate and phosphate concentrations were

observed south of the general region of Patch 2, closer to the South Georgia Island. Using the average strain rates from the SF_6 patch size ($0.1\sim0.2$ d^{-1}) and the north-south nutrient gradients, the lateral fluxes of nitrate and phosphate seem to be on the same order as the respective vertical fluxes. In contrast, silicate concentration was not enhanced in the south; thus horizontal mixing likely had little effect on its budget. In Patch 2, the silicate:nitrate ratio was 0.2 in ML and 0.6 below [*Lance et al.*, 2012]. The lower ratio of silicate:nitrate within the ML is also consistent with more nitrate horizontally mixed into the patch from the south.

References

Archer, S. D., F. J. Gilbert, J. I. Allen, J. Blackford J, and P. D. Nightingale (2004), Modelling of the seasonal patterns of dimethylsulphide production and fate during 1989 at a site in the North Sea, *Can. J. Fish. Aquat. Sci.*, *61*, 765–787.

Archer, S. D., et al. (2010), Dimethyl sulfoniopropionate and dimethyl sulfide production in response to photoinhibition in Emiliania huxleyi, *Limnol. Oceanogr.*, *55*, 1579–1589.

Archer, S. D., F. J. Gilbert, P. D. Nightingale, M. V. Zubkov, A. H. Taylor, G. C. Smith, and P. H. Burkill (2002), Transformation of dimethylsulphoniopropionate to dimethyl sulphide during summer in the North Sea with an examination of key processes via a modelling approach, *Deep Sea Res., Part II*, *49*(15), 3067–3101.

Arístegui, J., M. Denis, J. Almunia, and M. F. Montero (2002), Water-column remineralization in the Indian sector of the Southern Ocean during early spring, *Deep Sea Res., Part II*, *49*, 1707–1720.

Bailey, K. E., D. A. Toole, B. Blomquist, R. G. Najjar, B. Huebert, D. Kieber, R. Kiene, P. Matrai, G. R. Westby, and D. A. del Valle (2008), Dimethylsulfide production in Sargasso Sea eddies, *Deep Sea Res., Part II*, *55*, 1491–1504.

Bakker, D. C. E., et al. (2005) Iron and mixing affect biological carbon uptake in SOIREE and EisenEx, two Southern Ocean iron fertilisation experiments, *Deep Sea Res., Part I*, *52*, 1001–1019.

Bates, T. S., R. P. Kiene, G. V. Wolfe, P. A. Matrai, F. P. Chavez, K. R. Buck, B. W. Blomquist, and R. L. Cuhel (1994), The cycling of sulfur in surface seawater of the northeast Pacific, *J. Geophys. Res.*, *99*(C4), 7835–7843.

Bouillon, R., and W. L. Miller (2004), Determination of apparent quantum yield spectra of DMS photo-degradation in an in situ iron-induced Northeast Pacific Ocean bloom, *Geophys. Res. Lett.*, *31*, L06310, doi:10.1029/2004GL019536.

Boyd, P. W., et al. (2007), Mesoscale iron enrichment experiments 1993–2005: Synthesis and future directions, *Science*, *315*, 612–617.

Brimblecombe, P., and D. Shooter (1986), Photo-oxidation of dimethylsulphide in aqueous solution, *Mar. Chem.*, *19*, 343–353.

Charlson, R. J., J. E. Lovelock, M. O. Andreae, and S. G. Warren (1987), Oceanic phytoplankton, atmospheric sulfur, cloud albedo and climate, *Nature*, *326*, 655–661.

Charlson, R. J., S. E. Schwartz, J. M. Hales, R. D. Cess, J. A. Coakley Jr., J. E. Hansen, and D. J. Hoffman (1992), Climate forcing by anthropogenic aerosols, *Science*, *255*, 423–430.

Dacey, J. W., and S. G. Wakeham (1986), Oceanic dimethylsulfide: production during zooplankton grazing on phytoplankton, *Science*, *233*, 1314–1316.

Dacey, J. W. H., S. G. Wakeham, and B. L. Howes (1984), Henry's law constants for dimethylsulfide in freshwater and seawater, *Geophys. Res. Lett.*, *11*(10), 991–994.

Del Castillo, C. E., and R. L. Miller (2011), Horizontal and vertical distributions of colored dissolved organic matter during the Southern Ocean Gas Exchange Experiment, *J. Geophys. Res.*, *116*, C00F07, doi:10.1029/2010jc006781.

del Valle, D. A., D. J. Kieber, D. A. Toole, J. Brinkley, and R. P. Kiene (2009), Biological consumption of dimethylsulfide (DMS) and its importance in DMS dynamics in the Ross Sea, Antarctica, *Limnol. Oceanogr.*, *54*(3), 785–798.

Dickson, D. M. J., and G. O. Kirst (1986), The role of β-dimethylsulphoniopropionate, glycine betaine and homarine in the osmoacclimation of Platymonas subcordiformis, *Planta*, *167*, 536–543.

Goldson, L. (2004), Vertical mixing across the seasonal pycnocline of the Southern Ocean: Studies using sulphur hexafluoride tracer, PhD thesis, 219 pp., Univ. of East Anglia, Norwich, U. K.

Gregg, M. C. (1987), Diapycnal mixing in the thermocline: A review, *J. Geophys. Res.*, *92*, 5286–5429.

Hamme, R. C., et al. (2012), Dissolved O2/Ar and other methods reveal rapid changes in productivity during a Lagrangian experiment in the Southern Ocean, *J. Geophys. Res.*, *117*, C00F12, doi:10.1029/2011JC007046.

Hermann, M., et al. (2011), Diagnostic modeling of dimethylsulfide production in coastal water west of the Antarctic Peninsula, *Cont. Shelf Res.*, *32*, 96–109.

Ho, D. T., C. S. Law, M. J. Smith, P. Schlosser, M. Harvey, and P. Hill (2006), Measurements of air-sea gas exchange at high wind speeds in the Southern Ocean: Implications for global parameterizations, *Geophys. Res. Lett.*, *33*, L16611, doi:10.1029/2006GL026817.

Ho, D. T., C. L. Sabine, D. Hebert, D. S. Ullman, R. Wanninkhof, R. C. Hamme, P. G. Strutton, B. Hales, J. B. Edson, and B. R. Hargreaves (2011a), Southern Ocean gas exchange experiment: Setting the stage, *J. Geophys. Res.*, *116*, C00F08, doi:10.1029/2010JC006852.

Ho, D. T., R. Wanninkhof, P. Schlosser, D. S. Ullman, D. Hebert, and K. F. Sullivan (2011b), Toward a universal relationship between wind speed and gas exchange: Gas transfer velocities measured with 3He/SF6 during the Southern Ocean Gas Exchange Experiment, *J. Geophys. Res.*, *116*, C00F04, doi:10.1029/2010JC006854.

Keller, M. D., et al. (1989), Dimethylsulfide production in marine phytoplankton, in *Biogenic Sulfur in the Environment*, edited by E. Saltzman and W. J. Cooper, pp. 167–182, Am. Chem. Soc, Washington, D. C.

Kiene, R. P. (1990), Dimethyl sulfide production from dimethylsulfoniopropionate in coastal seawater samples and bacterial cultures, *Appl. Environ. Microbiol.*, *56*, 3292–3297.

Kiene, R. P., and T. S. Bates (1990), Biological removal of dimethyl sulphide from sea water, *Nature*, *345*, 702–705.

Kiene, R. P., and D. Slezak (2006), Low dissolved DMSP concentrations in seawater revealed by small-volume gravity filtration and dialysis sampling, *Limnol. Oceanogr. Methods*, *4*, 80–95.

Kiene, R. P., D. J. Kieber, D. Slezak, D. A. Toole, D. A. del Valle, J. Bisgrove, J. Brinkley, and A. Rellinger (2007), Distribution and cycling of dimethylsulfide, dimethyl-sulfoniopropionate, and dimethylsulfoxide during spring and early summer in the Southern Ocean south of New Zealand, *Aquat. Sci.*, *69*, 305–319.

Kiene, R. P., L. J. Linn, and J. A. Bruton (2000), New and important roles for DMSP in marine microbial communities, *J. Sea Res.*, *43*, 209–224.

King, D. B., and E. S. Saltzman (1995), Measurement of the diffusion coefficient of sulfur hexafluoride in water, *J. Geophys. Res.*, *100*, 7083–7088, doi:10.1029/94JC03313.

Lana, A., et al. (2011) An updated climatology of surface dimethlysulfide concentrations and emission fluxes in the global ocean, *Global Biogeochem. Cycles*, *25*, GB1004, doi:10.1029/2010GB003850.

Lance, V. P., P. G. Strutton, R. D. Vaillancourt, B. R. Hargreaves, J.-Z. Zhang, and J. Marra (2012), Primary productivity, new productivity, and their relation to carbon flux during two Southern Ocean Gas Exchange tracer experiments, *J. Geophys. Res.*, *117*, C00F14, doi:10.1029/2011JC007687.

Law, C. S., E. R. Abraham, A. J. Watson, and M. I. Liddicoat (2003), Vertical eddy diffusion and nutrient supply to the surface mixed layer of the Antarctic Circumpolar Current, *J. Geophys. Res.*, *108*(C8), 3272, doi:10.1029/2002JC001604.

Law, C. S., M. I. Liddicoat, A. J. Watson, and T. Stanton (1998), Sulphur hexafluoride as a tracer of biogeochemical and physical processes in an open-ocean iron fertilisation experiment, *Deep Sea Res.*, Part II, 45, 977–994.

Law, C. S., A. P. Martin, M. I. Liddicoat, A. J. Watson, K. J. Richards, and E. M. S. Woodward (2001), A Lagrangian SF6 tracer study of an

anticyclonic eddy in the North Atlantic: Patch evolution, vertical mixing and nutrient supply to the mixed layer, *Deep Sea Res., Part II*, *48*, 705–724.

Ledwell, J. R., A. J. Watson, and C.S. Law (1993), Evidence for slow mixing across the pycnocline from an open-ocean tracer-release experiment, *Nature*, *364*, 701–703.

Moore, T. S., M. D. DeGrandpre, C. L. Sabine, R. C. Hamme, C. J. Zappa, W. R. McGillis, R. A. Feely, and W. M. Drennan (2011), Sea surface pCO2 and O2 in the Southern Ocean during the austral fall, 2008, *J. Geophys. Res.*, *116*, C00F11, doi:10.1029/2010JC006560.

Nightingale, P. D., G. Malin, C. S. Law, A. J. Watson, P. S. Liss, M. I. Liddicoat, J. Boutin, and R. C. Upstill-Goddard (2000), In situ evaluation of air-sea gas exchange parameterizations using novel conservative and volatile tracers, *Global Biogeochem. Cycles*, *14*(1), 373–387, doi:10.1029/1999GB900091.

Orsi, A. H., T. Whitworth, and W. D. Nowlin (1995), On the meridional extent and fronts of the Antarctic Circumpolar Current, *Deep Sea Res., Part I*, *42*, 641–673, doi:10.1016/0967-0637(95)00021-W.

Polimene, L., S. D. Archer, M. Butenschön, and J. I. Allen (2012), A mechanistic explanation of the Sargasso Sea DMS "summer paradox", *Biogeochemistry*, *110*, 243–255, doi:10.1007/s10533-011-9674-z.

Simó, R., and J. Dachs (2002), Global ocean emission of dimethylsulfide predicted from biogeophysical data, *Global Biogeochem. Cycles*, *16*(4), 1078, doi:10.1029/2001GB001829.

Simó, R., and C. Pedrós-Alió (1999), Short-term variability in the open ocean cycle of dimethylsulfide, *Global Biogeochem. Cycles*, *13*, 1173–1182.

Smith, C. (2011), The relationship between phytoplankton pigment concentrations and DMSP, DMS and DMSO in a diatom-dominated bloom in the Ross Sea, Antarctica, Masters thesis, Univ. of South Alabama.

Smyth, T. J. (2011), Penetration of UV irradiance into the global ocean, *J. Geophys. Res.*, *116*, C11020, doi:10.1029/2011JC007183.

Smyth, T. J., G. F. Moore, T. Hirata, and J. Aiken (2006), Semianalytical model for the derivation of ocean color inherent optical properties: description, implementation, and performance assessment, *Appl. Opt.*, *45*(31), 8116–8131.

Stefels, J., and W. H. M. van Boekel (1993), Production of DMS from dissolved DMSP in axenic cultures of the marine phytoplankton species Phaeocystis sp., *Mar. Ecol. Prog. Ser.*, *97*, 11–18.

Sunda, W., D. J. Kieber, R. P. Kiene, and S. Huntsman (2002), An antioxidant function for DMSP and DMS in marine algae, *Nature*, *418*, 317–320.

Toole, D. A., D. J. Kieber, R. P. Kiene, D. A. Siegel, and N. B. Nelson (2003), Photochemistry and dimethylsulfide (DMS) summer paradox in the Sargasso Sea, *Limnol. Oceanogr.*, *48*, 1088–1110.

Toole, D. A., D. J. Kieber, R. P. Kiene, E. M. White, J. Bisgrove, D. A. del Valle, and D. Sleak (2004), High dimethylsulfide photochemistry rates in nitrate-rich Antarctic waters, *Geophys. Res. Lett.*, *31*, L11307, doi:10.1029/2004GL019863.

Toole, D. A., D. Slezak, R. P. Kiene, D. J. Kieber, and D. A. Siegel (2006), Effects of solar radiation on dimethylsulfide cycling in the western Atlantic Ocean, *Deep Sea Res., Part I*, *53*, 136–153.

Wanninkhof, R. (1992), Relationship between gas exchange and wind speed over the ocean, *J. Geophys. Res.*, *97*(C5), 7373–7382, doi:10.1029/92JC00188.

Wanninkhof, R., et al. (1997), Gas exchange, dispersion, and biological productivity on the west Florida shelf: Results from a Lagrangian tracer study, *Geophys. Res. Lett.*, *24*, 1767–1770.

Yang, M., B. W. Blomquist, C. W. Fairall, S. D. Archer, and B. J. Huebert (2011), Air-sea exchange of dimethylsulfide (DMS) in the Southern Ocean—Measurements from SO GasEx compared to temperate and tropical regions, *J. Geophys. Res.*, *116*, C00F05, doi:10.1029/2010JC006526.

Yang, M., B. W. Blomquist, and B. J. Huebert (2009), Constraining the concentration of the hydroxyl radical in a stratocumulus-topped marine boundary layer from sea-to-air eddy covariance flux measurements of dimethylsulfide, *Atmos. Chem. Phys.*, *9*, 9225–9236, doi:10.5194/acp-9-9225-2009.

Zubkov, M. V., B. M. Fuchs, S. D. Archer, R. P. Kiene, R. Amann, and P. H. Burkill (2002a), Rapid turnover of dissolved DMS and DMSP by defined bacterioplankton communities in the stratified euphotic zone of the North Sea, *Deep Sea Res., Part II*, *49*(15), 3017–3038, doi:10.1016/S0967-0645(02)00069-3.

Zubkov, M., L. J. Linn, R. Amann, and R. P. Kiene (2002b), Temporal patterns of biological dimethylsulfide (DMS) consumption during laboratory-induced phytoplankton bloom cycles, *Mar. Ecol. Prog. Ser.*, *271*, 77–86.